AGU PUBLICATIONS

Geophysical Research Letters

RESEARCH LETTER
10.1002/2015GL064534

Key Points:
- Several factors that limit shallow convection observation over land are described
- Every hour, forced and active cumuli size and cloud base dynamics are quantified
- Mixed-layer top velocity skewness and coherent updraft fraction most correlate to cumuli cover

Correspondence to:
K. Lamer,
katia.lamer@mail.mcgill.ca

Citation:
Lamer, K., and P. Kollias (2015), Observations of fair-weather cumuli over land: Dynamical factors controlling cloud size and cover, *Geophys. Res. Lett.*, *42*, 8693–8701, doi:10.1002/2015GL064534.

Received 11 MAY 2015
Accepted 1 JUL 2015
Accepted article online 2 JUL 2015
Published online 23 OCT 2015

Observations of fair-weather cumuli over land: Dynamical factors controlling cloud size and cover

Katia Lamer[1] and Pavlos Kollias[1]

[1]Department of Atmospheric and Oceanic Sciences, McGill University, Montreal, Québec, Canada

Abstract Comprehensive observations of shallow convection at the Atmospheric Radiation Measurement Southern Great Plains site are carefully analyzed to study the macrophysical and dynamical properties of active and forced cumuli separately and investigate their relationship to the subcloud layer turbulent structure. Clearly, active clouds possess stronger dynamics and greater horizontal extent than their forced counterpart. As previously reported, upper level stability and relative humidity do control the predominance of active clouds. While cloud cover remains difficult to associate to mixed-layer parameters (small correlation coefficients), mixed-layer top vertical velocity skewness, and coherent updraft fraction most significantly correlate to cumulus cloud cover and especially the portion attributed to active clouds; both of which are not currently considered in shallow cloudiness parameterizations. This study also points to several factors that continue to limit our ability to adequately sample shallow cumuli and suggests that forward models will be necessary to bridge observations and model outputs.

1. Introduction

Fair-weather cumuli often form over land during the warm season when surface thermals overshoot the lifting condensation level (forced cumuli). Less frequently do these thermals posses enough energy to develop significant vertical extent (active cumuli) [*Stull*, 1985]. Active cumuli exert a larger influence on the boundary layer evolution than their forced counterparts due to their ability to enhance the vertical transport of moisture, heat, and momentum [*Ahlgrimm and Forbes*, 2012]. Generally, the small size of cumulus clouds and their strong link to the subcloud layer complicate their representation in numerical models [e.g., *Lenderink et al*., 2004] as well as their holistic observation [e.g., *Chandra et al*., 2013].

The formation and vertical development of shallow cumuli is influenced by surface fluxes, boundary layer stability, and relative humidity [*Zhu and Albrecht*, 2003]. *Zhang and Klein* [2013; hereafter ZK13] observed the daily effect of boundary-layer thermodynamics on-cloud vertical extent and *Berg and Kassianov* [2008] on-cloud fraction both using the popular generic Active remote sensing of clouds Value-added product (VAP) [*Clothiaux et al*., 2001].

Boundary layer dynamics can be parameterized through mass flux and probability density function based schemes, which require some estimate of mixed-layer vertical velocity [e.g., *Bretherton et al*., 2004; *Lappen and Randall*, 2001; *Golaz et al*., 2002; *Sušelj et al*., 2012]. Large eddy simulations suggest that clouds are generated from the strongest subcloud layer updrafts, which are believed to be larger, undiluted, and most likely to penetrate the lifting condensation level [*Zhu and Albrecht*, 2003]. Yet the links between subcloud and cloud base dynamics as well as cloud extent have not been extensively documented by observational studies which tend to be limited to either the subcloud layer [e.g., *Ansmann et al*., 2010; *Miao et al*., 2006; *Chandra et al*., 2010; *Hogan et al*., 2009] or the cloud layer [e.g., *Chandra et al*., 2013]. This limitation can be attributed to the inability of any one conventional sensor to sample both mixed-layer and cloud layer air motion tracers (i.e., both aerosols and droplets) and/or to the presence of interfering targets (i.e., insects). This encourages the use of sophisticated instrument synergy to develop robust holistic observational statistics.

Eventually, all parameterizations schemes will have to rely on robust observational data sets from both island-based observing facilities [e.g., *Ghate et al*., 2011; *Lamer et al*., 2015; *Kollias and Albrecht*, 2010] and continental sites to evaluate their performance. The U.S. Department of Energy Atmospheric Radiation Measurement Program (ARM) Southern Great Planes site (SGP) is one of the best instrumented ground-based facilities and the recent designation of this site as a test bed for routine large eddy simulations prompts this study.

While not the first of its kind, the presented analysis differs in many ways. Here cumuli are treated as an ensemble of active and forced and each cloud-type characteristics are estimated separately every hour. The observational period, albeit short (2011–2014), has not been used in the past and contains information from a new suite of high-resolution sensors and VAPs. In short, the use of the SGP Doppler Lidar (DL) observations provides a wealth of information on the subcloud layer and cloud base dynamics and their relationship. Also, the radar used is more sensitive and the methodology for identifying insects above the cloud base height (CBH) is more comprehensive than any previous methodology. Finally, the infrequent soundings usually used to determine the thermodynamic structure of the boundary layer are substituted for the Raman lidar vertical profiles VAP and the merged-sounding VAP.

Despite the advantages provided by these sensors, observational limitations remain which are quantified in section 2.1. Section 3.1 discusses how deep (active) shallow cumuli are both bigger and more vigorous than their shallow (forced) counterparts. In section 3.2. we explain how boundary layer thermodynamics control the presence of active clouds, while subcloud dynamics are more significantly related to cloud cover (section 3.3). A summary of the main findings is provided in section 4 and a list of acronyms in section 5.

2. Observations and Challenges

The data used in this study were collected at the SGP Central facility located on 160 acres of cattle pasture and wheat fields southeast of Lamont, Oklahoma [*Stokes and Schwartz*, 1994; *Mather and Voyles*, 2013]. All instruments presented below are located within 100 m of each other such that their synergistic use is reasonable [*Chandra et al*., 2013]. Note that all data beyond 5 km height are disregarded.

1. Ceilometer cloud base detections collected every 16 s are used to isolate individual clouds, determine their duration, and produce hourly-averaged estimates of cloud cover (CC) defined as the fraction of time in an hour where clouds are overhead and CBH.
2. The Merged-sounding VAP horizontal wind speed profiles [*Troyan*, 2012] are averaged hourly and interpolated to the DL range resolution in order to convert observed time overhead the sensors to horizontal distance (i.e., chord length).
3. The convective velocity scale (w^*) is estimated according to *Stull* [1988] using hourly surface flux estimates from the Energy balance Bowen ratio system.
4. Individual cloud maximum liquid water path (LWP) is extracted from the Microwave radiometer (MWR) 30 s resolution LWP series adjusted to ensure zero hourly-averaged clear sky LWP.
5. Hourly-averaged profiles of virtual potential temperature (θ_v) based on the Raman lidar vertical profiles VAP (75 m vertical resolution; https://www.arm.gov/data/vaps/rlprof/10rlprofbe1turn) are used to determine mixed-layer top height (MLH) defined as the maximum height below CBH where $d\theta_v/dz$ is less than 0.75 K km^{-1}. In addition, the environmental stability defined as the gradient of potential temperature 300 m above the highest cloud top is estimated and so is the mixed-layer mean relative humidity.
6. Zenith DL observations of vertical velocity are available at a temporal resolution of 1.2 s and range resolution of 30 m. Noise present in this data set is filtered in two steps: First, data with signal-to-noise ratio below 1 are removed, then, every three consecutive DL range gates, observations beyond five standard deviations of the mean are also filtered out. Subsequently, the moments of the vertical velocity field are estimated (1) for each cloud at the closest range gate to the CBH, (2) hourly at the MLH (3) for each nonnegligible coherent structure in the mixed layer. Coherent structures in the mixed layer are isolated using a velocity threshold of 0.1 meters per second (m s^{-1}) as in *Ansmann et al*. [2010]. For each structure, horizontal extent is estimated every range gate, while vertical extent is estimated every time step. Consequently, only the maximum extents are used to identify structures of interest (structure with extents larger than 5% CBH).
7. A significant feature (i.e. insects, clouds, and precipitation) mask is generated for the Ka-band ARM Zenith Radar (KAZR) 3.7 s, 30 m resolution observations using the *Hildebrand and Sekhon* [1974] technique. Using the ceilometer as an adamant indicator of the location of clouds, significant radar features below and between ceilometer returns can be labeled as insects. Moreover, for hours where insect layers are present between clouds at cloud level, all radar echoes are deemed suspicious and classified as inside insect layers. For all remaining radar features, above every ceilometer cloud base, the highest echo is used to estimate the cloud top height and cloud top reflectivity.

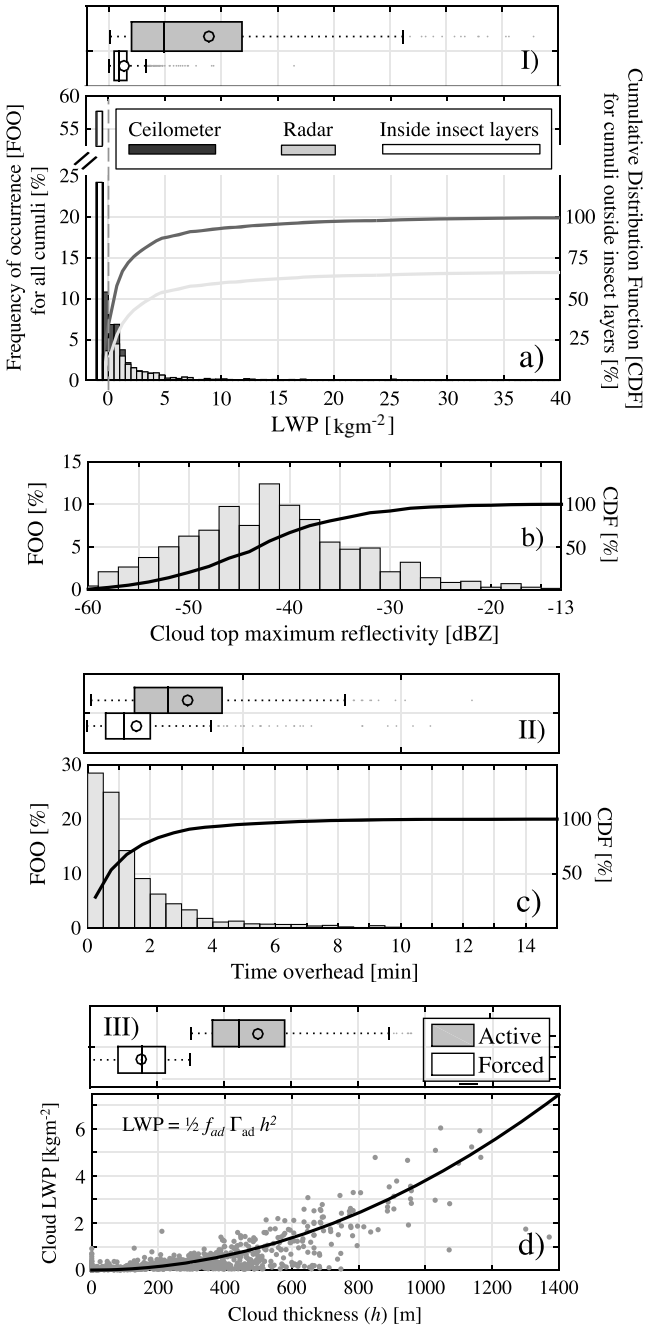

Figure 1. Statistics for individual cumuli. (a) LWP frequency of occurrence (FOO) for all clouds as observed by the ceilometer (black) and portion of clouds observed by the radar (grey). Also indicated are clouds buried in insect layers (white) and clouds undetected by the microwave radiometer (negative LWP). The figure includes cumulative distribution functions (CDF) for clouds outside insect layers (lines). (b) Cloud top maximum reflectivity FOO (bar). (c) Overpass time FOO (bar); both including CDF (line). (d) Scatter of cloud thickness versus LWP including an adiabatic estimate. Subpanels I–III are statistics for the active (dark grey) and forced (white) cloud groups. The circle marks the mean, the box indicates the interquartile range surrounding the median line, whiskers extend to the 5th and 95th percentiles, extreme values if any are plotted as dots.

2.1. Challenges in Observing Shallow Cumuli at the SGP

This study focuses on the summer (May–September), daytime periods of 2011–2013 and partially 2014. Five criteria are used to select fair-weather cumulus hours: (1) CC 3–60%, (2) lack of stratiform clouds (cloud duration $<$ 20 min), (3) absence of rain (reflectivity $<$ 0 dBZ), (4) absence of deep convection (cloud top $<$ 4 km), and (5) absence of insects above CBH. The ceilometer and KAZR are used to test these criteria every hour below 5 km height.

In total, 525 h satisfy the first four criteria. Unfortunately, not all 525 h (3461 cumuli) are suitable for further analysis. Insects flying above the CBH (fifth criteria) may create fictitiously high cloud tops in 59% of the cumuli observed by the radar (Figure 1a white bar). The omnipresence of insects in the boundary layer at the SGP was previously documented [*Chandra et al.*, 2013; *Luke et al.*, 2008] but is worth mentioning again due to its profound implications for shallow cloud studies. Besides cloud top, insects may affect radar reflectivity and Doppler velocity throughout the lowest part of the clouds as indicated by a subset of KAZR linear depolarization ratio observations (not shown) and that even if "insect cases" are filtered. As such, we advice that future analyses estimating air motion, microphysical quantities, or even cloud aspect ratio using cloud radar observations should be conducted with diligence.

The 1401 cumuli outside insect layers have low reflectivity due to their small droplet sizes characteristic of polluted continental clouds, which further impedes their detection by KAZR. The KAZR (Figure 1a light grey line) reports no hydrometeor echoes in 37% of these ceilometer-detected clouds (Figure 1a black line). A histogram of the maximum cloud top reflectivity of the 882 cumuli observed by the KAZR reveals that any radar with a sensitivity below −43 dBZ at 2 km would miss to observe

Table 1. Hourly Cloud Characteristics and Correlations (*R*) to Cloud Thickness[a]

	12:00-14:00		14:00-16:00		16:00-18:00		
	Active cumuli	Forced cumuli	Active cumuli	Forced cumuli	Active cumuli	Forced cumuli	
	median *IQR*	*median* *IQR*	*median* *IQR*	*median* *IQR*	*median* *IQR*	*median* *IQR*	
Occurence - all cumuli (hrs)	69		91		76		
Occurrence (hrs)	44	65	61	81	33	71	
Cloud cover - all cumuli (%)	11.9 6.9/20.3		14.2 7.6/27.9		10.9 5.1/21.4		
Contributon to cloud cover - when occuring concurrently (%)	62.7 47.2/74.4	37.3 25.6/52.8	66.9 48.0/79.9	33.1 20.1/52.0	64.8 49.8/81.7	36.2 18.3/50.2	**Correlation coefficients (R) relative to cloud thickness**
Cloud thickness - when detected by radar (m)	481 389/545	176 124/203	429 380/517	158 116/206	510 378/613	143 104/179	
Cloud aspect ratio (Depth/Length) - when detected by radar	0.61 0.36/0.84	0.34 0.21/0.61	0.48 0.32/0.62	0.26 0.19/0.54	0.39 0.31/0.51	0.21 0.13/0.38	
Cloud base							
Cloud chord length (m)	820 650/1428	397 270/624	1070 803/1438	384 252/629	1548 988/2100	484 293/745	
Cloud base height (km)	2.04 1.69/2.51	2.27 1.78/2.61	2.26 1.88/2.65	2.47 1.95/2.78	2.05 1.81/2.69	2.28 1.86/2.77	
Mean updraft velocity (ms^{-1})	0.97 0.6/1.34	0.58 0.36/0.80	0.99 0.72/1.48	0.62 0.46/0.88	0.70 0.55/1.00	0.54 0.39/0.75	0.34
Mean downdraft velocity (ms^{-1})	0.84 0.55/1.06	0.62 0.49/0.81	0.71 0.58/0.86	0.66 0.49/0.81	0.62 0.52/0.81	0.54 0.42/0.70	0.13
Maximum updraft velocity (ms^{-1})	3.13 1.78/4.07	1.41 0.90/2.20	3.15 2.10/4.41	1.65 1.13/2.32	2.27 1.41/2.89	1.31 0.94/1.85	0.41
Maximum downdraft velocity (ms^{-1})	2.63 1.90/3.39	1.63 1.17/2.25	2.39 1.78/2.92	1.72 1.21/2.26	2.50 1.62/2.81	1.39 1.04/1.99	0.27
In-cloud updraft fraction (%) [In-cloud downdraft fraction = 100-X%]	52.0 43.8/65.0	42.3 29.5/54.4	53.9 45.7/68.8	45.7 30.5/56.5	53.3 36.8/61.2	46.1 29.2/58.9	0.15

[a]Results that fail a 95% (90%) Student *t* test are marked by a diagonal line (X mark).

another 50% of the nonprecipitating cumulus field at the SGP (Figure 1b). This adds considerable challenges for off-zenith (three-dimensional) cloud observations using scanning cloud radars [*Lamer et al.*, 2013; *Kollias et al.*, 2014].

Furthermore, the limited time these clouds spend overhead profiling instruments creates a possible partial-beam filling issue for the MWR (5° beam width ≈ 30 s sampling frequency). Twenty-seven percent of the cumuli sampled by the ceilometer are overhead for less than 30 s (Figure 1c). This could explain why the MWR cannot report reliable LWP for 25% of the cumulus cases outside insect layer (Figure 1a on the negative *x* axis).

Despite the aforementioned challenges, 1401 cumuli are analyzed here. A scatterplot of cloud thickness versus LWP is shown in Figure 1d. The observations scatter around an average liquid water content adiabatic rate of increase of 1.4 g m^{-3} km^{-1} (Γ_{adi}) and a 0.4° of adiabaticity (f_{adi}) [*Wood*, 2006].

3. Results

3.1. The Differences of Active and Forced Cumuli

Unlike to previous studies, each hour is considered as a possible ensemble of forced clouds, merely neutral thermal overshoots, and buoyant active clouds able to generate secondary circulations and enhanced boundary layer mixing. As such, each individual cloud within an hour is classified using a thickness threshold of 300 m; active clouds being deeper than this threshold and forced clouds shallower. This technique is similar to the daily classification proposed by ZK13 and a sensitivity study was conducted to ensure its suitability to the finer temporal resolution data used here. Also, ceilometer-detected clouds undetected by the radar are assumed to be shallow and are classified as forced. Each hour, once the characteristics of every cloud are determined, the hourly-mean characteristics of each cloud type are computed. The hourly statistics are aggregated in three time periods for which we display the quartiles. In addition, Student *t* statistics are used to test if active clouds are significantly different from the main population (forced; Table 1).

Unlike forced cumuli (41.5% of the time), active cumuli rarely (8% of the time) present themselves as the only form of convection. The remaining 50.5% of the time active cumuli form alongside forced cumuli. This mixture of cumulus types creates a fairly stable median CC around 12.5%, highest (14.2%) at 15:00. When occurring concurrently active clouds contribute 65% of the CC and thus more than forced clouds, which could be explained by their larger chord length. The chord length of the forced cumuli is fairly constant 384–484 m while that of active cumuli increase throughout the day from 820 to 1548 m. In addition, on average, the radar detected active clouds are three times as thick as their forced counterpart (473 versus 159 m, respectively). Cumulus aspect ratio, depth over length, reduced over the course of the afternoon starting about 0.34/0.61 (forced/active) and ending about 0.21/0.39; Even though active clouds systematically have higher aspect ratio both cumulus types have ratio below one indicating pancake like clouds. These figures differ significantly from previous SGP cumulus studies that report active cumuli with aspect ratio about 2 [*Chandra et al.*, 2013; ZK13]. Such results could only be reproduced if considering all echoes above ceilometer as clouds and as such ignoring the presence of invasive insect layers.

The cumuli at SGP form a little more than 100 m above the MLH within the inversion layer. On average active cumuli tend to form 223 m lower than forced cumuli hinting to their preference for moister boundary layers. At CBH, their velocity statistics differ significantly. Note that these differences are more pronounced in early afternoon and diminish over the course of the day (Table 1). Updrafts cover 8–10% more area in active clouds. The differences in mean updraft/downdraft velocity between active and forced cumuli are larger during 12:00–16:00 (1.0/−0.8 and 0.6/−0.6 m s^{-1}, respectively). Also, maximum velocities amplitudes are at least of 40% larger in active clouds. Examination of the diurnal cycle of each cumulus type indicates that active cumuli maintain the strength of their updrafts through 16:00 which then lose intensity drastically (in a way similar to w^*), while their downdrafts are stronger around 13:00 and lose intensity slowly during the day. Alternatively, forced cumuli draft intensity remains very stable and is of similar amplitude for up and down motions. Finally, all clouds considered, maximum updraft velocity is found to have the largest correlation to thickness ($R = 0.41$) but no attempt is made here to use this parameter to infer thickness [*Zheng et al.*, 2015].

3.2. Factors Controlling the Formation of Active Clouds

In an attempt to predict the presence of active clouds from environmental conditions, hours without active clouds are averaged to capture the forced cumuli environmental characteristics (white columns) while hours where at least one third of the customary CC (i.e., 5%) can be attributed to the presence of active clouds are averaged to capture the active cumuli environmental conditions (shaded columns) (Table 2). Once again, quartiles are displayed for each 3 h group and Student t statistics are be used to determine if the active set is significantly different than the forced set.

As was previously acknowledged, the environmental stability is ~2 K km^{-1} smaller when active clouds form (ZK13). Environmental stability varies around 4/6 K km^{-1} (active/forced) with it largest value 5/7 K km-1 about 15:00. Another result in agreement with literature is a 4–6% mixed-layer relative humidity enhancement when active clouds are detected which is consistent with the observed CBH differences.

Sensible heat flux (SHF) values do not change significantly across the different shallow convection modes. Alternately, smaller latent heat flux (LHF) around 15:00 is observed for active cloud periods. Despite the relatively similar fluxes associated to active and forced cumuli, their median Bowen ratios show significant differences as well as large variability during the day (for forced clouds: 2.9, 1.7, and 1.0 at 13:00, 15:00, and 17:00, respectively), which follows from the SHF reaching its maximum value at 13:00, while the LHF at 15:00. What is more, w^* daytime evolution follows that of the SHF. Also at 15:00 and 17:00 w^* during active cumuli is found to be significantly higher than that reported for forced cumulus periods.

Most vertical velocity statistics estimated at the MLH have very little skill at predicting the presence of active cumuli. The significant quantities for active clouds: higher updraft fraction (at 13:00; 39 versus 35%), lower mean downdraft velocity (at 15:00, 0.59 versus 0.69 m s^{-1}), higher skewness (at 15:00, 0.90 versus 0.76), higher mean updraft velocity (at 17:00, 0.55 versus 0.50 m s^{-1}), Even if insignificantly different, all other reported quantities are useful for model validation. If we explore their diurnal cycle, MLH updrafts maintain their strength from 13:00 to 16:00 then weaken while downdraft strength reduces progressively throughout the afternoon. These trends are similar to the ones observed at the base of active clouds. In the same spirit, updraft fraction temporal variations are on the order of 3%. Lastly, MLH skewness is

Table 2. Environmental Factors for Active Periods (Active Cumulus Cover > 5%) and Forced Periods (Active Cumulus Cover = 0%)[a]

	12:00-14:00		14:00-16:00		16:00-18:00	
	Active periods	Forced periods	Active periods	Forced periods	Active periods	Forced periods
	median *IQR*	*median* *IQR*	*median* *IQR*	*median* *IQR*	*median* *IQR*	*median* *IQR*
Surface						
Occurrence (hrs)	38	25	50	30	29	43
Convective velocity scale (ms^{-1})	2.81 2.30/2.98	2.83 2.38/3.10	2.74 2.13/3.08	2.54 2.20/2.86	2.13 1.69/2.66	2.05 1.68/2.41
Sensible heat flux (Wm^{-2})	368.1 236.6/453.7	419.7 230.6/447.7	292.6 200.2/407.3	309.9 167.1/375.4	164.6 82.9/263.2	130.3 100.4/221.0
Latent heat flux (Wm^{-2})	115.3 64.3/236.4	144.5 81.0/230.4	166.0 72.7/284.0	200.6 143.4/299.4	188.9 83.6/282.3	156.9 102.1/258.2
Mixed-layer						
Mean relative humidity (%)	60.5 53.4/70.4	54.9 47.8/66.0	59.0 54.3/62.5	54.6 49.8/60.2	61.1 55.5/68.0	56.9 52.1/65.7
300 m above cloud top						
Environment stability (Kkm^{-1})	4.4 2.9/7.2	5.8 3.9/8.9	5.1 3.8/7.1	7.1 5.1/8.4	3.9 3.0/5.57	6.2 5.1/8.0
Mixed-layer top						
Mixed-layer top height (km)	2.14 1.62/2.52		2.14 1.84/2.59		2.14 1.69/2.67	
Mean updraft velocity (ms^{-1})	0.66 0.50/0.87	0.68 0.44/0.81	0.68 0.56/0.81	0.65 0.54/0.93	0.55 0.47/0.72	0.50 0.40/0.65
Mean downdraft velocity (ms^{-1})	0.60 0.52/0.75	0.61 0.50/0.67	0.59 0.53/0.66	0.69 0.59/0.77	0.57 0.49/0.65	0.56 0.50/0.62
Updraft fraction (%)	38.6 33.4/44.0	35.4 31.5/40.1	36.1 33.2/40.7	35.6 33.3/39.8	34.6 31.2/41.5	37.5 31.9/40.7
Penetrating coherent updraft fraction (%)	18.0 11.5/27.6	7.2 3.8/15.7	17.9 11.5/22.8	14.2 8.4/26.4	17.2 10.7/22.2	18.2 11.6/25.5
Velocity variance (ms^{-1})	0.83 0.47/1.00	0.67 0.42/1.26	0.70 0.58/0.99	0.89 0.62/1.34	0.53 0.36/0.90	0.46 0.36/0.72
Velocity skewness	0.79 0.33/1.18	0.65 0.32/1.18	0.90 0.51/1.21	0.76 0.41/0.98	0.41 0.26/0.87	0.43 0.22/0.74

[a]Results that fail a 95% (90%) Student *t* test are marked by a diagonal line (X mark).

largest at 15:00 and smallest at 17:00 [*Chandra et al.*, 2010]. Note that the amplitudes reported by *Chandra et al.* [2010] are much smaller (~ −0.2–0.3 versus ~ 0.4–0.9), this could be attributed to their using adjusted insect motion for air motion. Given that the magnitude we report is consistent with other DL studies [*Ansmann et al.*, 2010; *Hogan et al.*, 2009], we advice to hold off from using insects to derive high-order statistics of the vertical air motion field.

In addition to MLH statistics considering all vertical motions, the role of vertical velocity coherent structures in the subcloud layer is investigated. In particular, the coverage of penetrating clear-air coherent structures at the MLH is estimated. By penetrating we mean the ones with base within the mixed layer and top above the mixed layer. It appears that during early afternoon hours, periods with higher penetrating coherent updraft fraction at the MLH contain active clouds (Table 2). Not only this but a clear relationship between the size of the coherent structures and their mean vertical velocity is found (Figure 2). Wider or deeper coherent structures contain higher mean vertical velocities. This suggests that wider coherent structures are more likely to form active clouds [*Zhu and Albrecht*, 2003]. This is also in agreement with the observed differences in cloud chord length and mean updraft velocity of active and forced clouds (grey and white whisker boxes, Figure 2a). Besides this, updrafts of the same horizontal or vertical extent contain higher magnitude velocities than their downdraft counterparts (Figure 2 blue and red solid lines) [*Ansmann et al.*, 2010]. This is consistent with the positive skewness of the vertical velocity field throughout the subcloud layer. About 80% of the coherent updraft structures have width normalized by CBH 0.25 or less (Figure 2a blue dashed line). This result, even if sensitive to the criteria used to isolate drafts, compares well with previous aircraft observational studies that found exponential [*Miao et al.*, 2006]

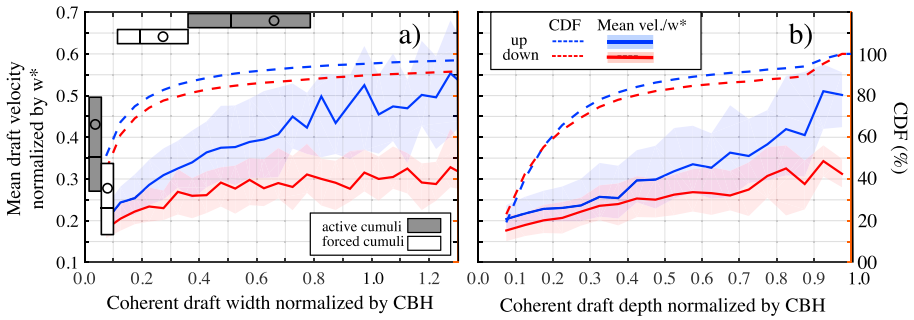

Figure 2. Statistics of coherent updrafts (blue) and downdrafts (red) (a) Cumulative distribution function of coherent draft width normalized by cloud base height (CBH) (dashed lines; right-hand side *Y* axis) and relationship with mean draft velocity normalized by *w** (solid lines: median/shading: Interquartile range; left-hand side *Y* axis). Also included are statistics of cumuli: chord length normalized by CBH (horizontal boxes) and mean updraft velocity at cloud base normalized by *w** (vertical boxes; same display as Figure 1). (b) Using depth rather than width.

or lognormal [*Greenhut and Singh Khalsa*, 1982; *Young*, 1988] plume width distributions. Similarly, 80% of them have depth normalized by CBH 0.35 or less (Figure 2b blue dashed line). In addition, we find a strong preference for coherent updraft structures to originate near the surface (~36%) and vanish above the MLH (~17%; not shown) the same can be said for downdraft coherent structures which is consistent with long-standing understanding of the boundary layer structure.

3.3. Factors Controlling Cloud Cover

Here correlative relationships are compute between (1) hourly total CC (light grey column), (2) the portion due to active cumuli (dark grey) when present, and (3) forced cumuli (white) when present against a number of surface, mixed-layer and MLH thermodynamic and dynamic parameters (Table 3). *P* values are used to determine the significance of the correlations.

While the surface heat fluxes are not significantly correlated with CC, *w** is negatively correlated with the active and forced CC but not significantly with the total CC suggesting that different modes of shallow convection posses different relationships to the surface. Above the surface, the mixed-layer mean relative humidity is positively related to the total CC, however, this relationship breaks down if CC is separated into its components. Alternatively, environmental stability positively relates to all portions of the CC, which suggests that the more stable the environment the higher the cumulus cover is no matter what the mode of convection is.

At the MLH, mean downdraft velocity and velocity variance have little to no skill at predicting CC. The better parameters are, in decreasing order: Penetrating coherent updraft fraction ($R_{active} = 0.32$), velocity skewness ($R_{active} = 0.28$), mean updraft velocity ($R_{active} = 0.23$), and updraft fraction ($R_{active} = 0.20$). All correlations are stronger with the active CC than with either the total or forced CC yet none of the correlations exceed 0.32, which reinforced the idea that cumulus clouds are controlled by a large set of parameters.

4. Summary

This study introduces for first time a breakdown of hourly cloud cover (CC) into its active and forced shallow cumulus components and treats each cloud type separately. This separation is undertaken based on the hypothesis that these different fair-weather cumulus types result from different subcloud layer processes and generate different cloud circulations. The nearly constant CC at SGP (~12.5%) is created by an ensemble of active and forced clouds more frequently (58–56%) during early afternoon and less frequently (36%) during late afternoon when forced clouds tend to be the preferred mode of convection. Active cumuli are 2–3 times wider. This agrees well with our finding that wider subcloud layer coherent structures contain stronger updrafts. It is evident that active clouds are more vigorous and their updrafts and downdrafts are not in balance. Ultimately, the thermodynamic structure of the boundary layer dictates the mode of convection: Larger (4–6%) mixed-layer averaged relative humidity and smaller (2 K km^{-1}) upper level (300 m above cloud top) environmental stability are observed during

Table 3. Correlation Coefficients (*R*) Relative to Hourly Total Cloud Cover [CC] and to the Breakdown Between Active and Forced Cumuli Cloud Cover When Present[a]

	Correlation coefficients (R)		
	Total CC	Active CC	Forced CC
Surface			
Convective velocity scale	~~0.08~~	-0.19	-0.16
Sensible heat flux	~~0.01~~	~~0.13~~	~~0.08~~
Latent heat flux	~~0.05~~	~~0.03~~	~~0.05~~
Mixed-layer			
Mean relative humidity	~~0.12~~	~~0.11~~	~~0.05~~
Above cloud top			
Environmental stability	0.10	0.18	~~0.17~~
Mixed-layer top			
Mean updraft velocity	0.21	0.23	~~0.07~~
Mean downdraft velocity	~~0.02~~	~~0.07~~	~~0.05~~
Updraft fraction	0.18	0.20	0.18
Penetrating coherent updraft fraction	0.31	0.32	0.19
Velocity variance	~~0.10~~	~~0.10~~	~~0.06~~
Velocity skewness	0.26	0.28	~~0.12~~

[a]Results with *p* value greater than 5% (10%) are marked by a diagonal line (X mark).

active clouds periods. While the dynamic structure of the mixed layer is very similar regardless of the presence or absence of active cumuli its characteristics vary according to CC. Updraft fraction (0.2) and updraft velocity (0.2) as well as vertical velocity skewness (0.3) and coherent updraft fraction (0.3) at the MLH significantly correlate to CC and especially the portion attributed to active clouds when they are present. The latter two parameters are not currently considered in shallow cloudiness parameterizations. These weak correlations suggest that the parameterization of shallow cumulus cloud is challenging. The inclusion of additional parameters could improve the prediction of fair-weather cumulus properties, however, future studies are required to quantify their value.

The current study also raises significant concerns about our ability to characterize the full fair-weather cumulus population at the SGP and its outcome will influence the final configuration of the SGP megasite. While lidars can provide reliable subcloud and cloud base measurements, the same cannot be said for all microwave sensors. The LWP from the MWR is underestimated in 25% of the cumuli outside insect layers due to nonuniform beam filling. In addition, the presence of insects and the low radar reflectivity of cumuli pose a considerable detection challenge for the radar especially at the SGP a continental site where droplet sizes are expected to be small and where insects are present near and above cloud base. Insects are bias tracers of air motion and more fundamentally, if misclassified for clouds they can create cloud thickness bias. We determined that only 25% of the clouds detected by the ceilometer can be properly sized by the KAZR. All these complications suggest that continental observation and model output intercomparisons would require careful conditional sampling using instrument forward models. Nevertheless, the statistics provided in this study provide robust observational targets for continental shallow convection modeling studies.

5. List of Acronyms

ARM Atmospheric radiation measurement program
CBH Cloud base height
CC Cloud cover
DL Doppler lidar
KAZR Ka-band ARM zenith radar
LHF Latent heat flux
LWP Sensible heat flux
MLH Mixed-layer top height

MWR	Microwave radiometer
SGP	Southern great planes site
SHF	Sensible heat flux
VAP	Value-added product
ZK13	*Zhang and Klein* [2013]

Acknowledgments

The current research was supported by the Department of Energy Atmospheric System Research program. We would like to thank our reviewers and the McGill Clouds Group for their constructive comments. The data sets used in this study can be downloaded on the ARM website: http://www.archive.arm.gov/armlogin/login.jsp. The list of case studies used to derive cumuli characteristics outside insect layers can be obtained by contacting the main author.

The Editor thanks two anonymous reviewers for their assistance in evaluating this paper.

References

Ahlgrimm, M., and R. Forbes (2012), The impact of low clouds on surface shortwave radiation in the ECMWF model, *Mon. Weather Rev.*, *140*(11), 3783–3794.

Ansmann, A., J. Fruntke, and R. Engelmann (2010), Updraft and downdraft characterization with Doppler lidar: Cloud-free versus cumuli-topped mixed layer, *Atmos. Chem. Phys.*, *10*(16), 7845–7858.

Berg, L. K., and E. I. Kassianov (2008), Temporal variability of fair-weather cumulus statistics at the ACRF SGP site, *J. Clim.*, *21*(13), 3344–3358.

Bretherton, C. S., J. R. McCaa, and H. Grenier (2004), A new parameterization for shallow cumulus convection and its application to marine subtropical cloud-topped boundary layers. Part I: Description and 1D results, *Mon. Weather Rev.*, *132*(4), 864–882.

Chandra, A. S., P. Kollias, S. E. Giangrande, and S. A. Klein (2010), Long-term observations of the convective boundary layer using insect radar returns at the SGP ARM climate research facility, *J. Clim.*, *23*(21), 5699–5714.

Chandra, A. S., P. Kollias, and B. A. Albrecht (2013), Multiyear summertime observations of daytime fair-weather cumuli at the arm southern great plains facility, *J. Clim.*, *26*, 10,031–10,050, doi:10.1175/JCLI-D-12-00223.1.

Clothiaux, E. E., M. A. Miller, R. C. Perez, D. D. Turner, K. P. Moran, B. E. Martner, T. P. Ackerman, G. G. Mace, R. T. Marchand, and K. B. Widener (2001), *The ARM Millimeter Wave Cloud Radars (MMCRs) and the Active Remote Sensing of Clouds (ARSCL) Value Added Product (VAP)*, Pacific Northwest Natl. Lab.

Ghate, V. P., M. A. Miller, and L. DiPretore (2011), Vertical velocity structure of marine boundary layer trade wind cumulus clouds, *J. Geophys. Res.*, *116*, D16206, doi:10.1029/2010JD015344.

Golaz, J.-C., V. E. Larson, and W. R. Cotton (2002), A PDF-based model for boundary layer clouds. Part I: Method and model description, *J. Atmos. Sci.*, *59*(24), 3540–3551.

Greenhut, G. K., and S. J. Singh Khalsa (1982), Updraft and downdraft events in the atmospheric boundary layer over the equatorial Pacific Ocean, *J. Atmos. Sci.*, *39*(8), 1803–1818.

Hildebrand, P. H., and R. S. Sekhon (1974), Objective determination of the noise level in Doppler spectra, *J. Appl. Meteorol.*, *13*(7), 808–811.

Hogan, R. J., A. L. Grant, A. J. Illingworth, G. N. Pearson, and E. J. O'Connor (2009), Vertical velocity variance and skewness in clear and cloud-topped boundary layers as revealed by Doppler lidar, *Q. J. R. Meteorol. Soc.*, *135*(640), 635–643.

Kollias, P., and B. Albrecht (2010), Vertical velocity statistics in fair-weather cumuli at the ARM TWP Nauru Climate Research Facility, *J. Clim.*, *23*(24), 6590–6604.

Kollias, P., N. Bharadwaj, K. Widener, I. Jo, and K. Johnson (2014), Scanning ARM cloud radars. Part I: Operational sampling strategies, *J. Atmos. Oceanic Technol.*, *31*(3), 569–582.

Lamer, K., A. Tatarevic, I. Jo, and P. Kollias (2013), Evaluation of gridded Scanning ARM Cloud Radar reflectivity observations and vertical Doppler velocity retrievals, *Atmos. Meas. Tech. Discuss.*, *6*, 9579–9621.

Lamer, K., P. Kollias, and L. Nuijens (2015), Observations of the variability of shallow trade-wind cumulus cloudiness and mass flux, *J. Geophys. Res. Atmos.*, *120*, doi:10.1002/2014JD022950.

Lappen, C.-L., and D. A. Randall (2001), Toward a unified parameterization of the boundary layer and moist convection. Part I: A new type of mass-flux model, *J. Atmos. Sci.*, *58*(15), 2021–2036.

Lenderink, G., A. Siebesma, S. Cheinet, S. Irons, C. G. Jones, P. Marquet, F. M. üLLER, D. Olmeda, J. Calvo, and E. Sánchez (2004), The diurnal cycle of shallow cumulus clouds over land: A single-column model intercomparison study, *Q. J. R. Meteorol. Soc.*, *130*(604), 3339–3364.

Luke, E. P., P. Kollias, K. L. Johnson, and E. E. Clothiaux (2008), A technique for the automatic detection of insect clutter in cloud radar returns, *J. Atmos. Oceanic Technol.*, *25*(9), 1498–1513.

Mather, J. H., and J. W. Voyles (2013), The ARM Climate Research Facility: A review of structure and capabilities, *Bull. Am. Meteorol. Soc.*, *94*(3), 377–392.

Miao, Q., B. Geerts, and M. LeMone (2006), Vertical velocity and buoyancy characteristics of coherent echo plumes in the convective boundary layer, detected by a profiling airborne radar, *J. Appl. Meteorol. Climatol.*, *45*(6), 838–855.

Stokes, G. M., and S. E. Schwartz (1994), The Atmospheric Radiation Measurement (ARM) Program: Programmatic background and design of the cloud and radiation test bed, *Bull. Am. Meteorol. Soc.*, *75*(7), 1201–1221.

Stull, R. B. (1985), A fair-weather cumulus cloud classification scheme for mixed-layer studies, *J. Climate Appl. Meteorol.*, *24*(1), 49–56, doi:10.1175/1520-0450(1985)024<0049:AFWCCC>2.0.CO;2.

Stull, R. B. (1988), *An Introduction to Boundary Layer Meteorology*, vol. 13, Springer Science and Business Media.

Sušelj, K., J. Teixeira, and G. Matheou (2012), Eddy diffusivity/mass flux and shallow cumulus boundary layer: An updraft PDF multiple mass flux scheme, *J. Atmos. Sci.*, *69*(5), 1513–1533.

Troyan, D. (2012), Merged sounding value-added product, *DOE-ARM Tech. Rep.*, *DOE/SC-ARM/TR-087*.

Wood, R. (2006), Relationships between optical depth, liquid water path, droplet concentration, and effective radius in adiabatic layer cloud, pp. 3, Univ. of Washington.

Young, G. S. (1988), Turbulence structure of the convective boundary layer. Part II. Phonenix 78 aircraft observations of thermals and their environment, *J. Atmos. Sci.*, *45*(4), 727–735.

Zhang, Y., and S. A. Klein (2013), Factors controlling the vertical extent of fair-weather shallow cumulus clouds over land: Investigation of diurnal-cycle observations collected at the ARM Southern Great Plains site, *J. Atmos. Sci.*, *70*(4), 1297–1315.

Zheng, Y., D. Rosenfeld, and Z. Li (2015), Satellite inference of thermals and cloud base updraft speeds based on retrieved surface and cloud base temperatures, *J. Atmos. Sci.*, *72*, 2411–2428.

Zhu, P., and B. Albrecht (2003), Large eddy simulations of continental shallow cumulus convection, *J. Geophys. Res.*, *108*(D15), 4453, doi:10.1029/2002JD003119.